Propulsion and Power Research 2024;13(1):12–25

http://ppr.buaa.edu.cn/

Propulsion and Power Research

www.sciencedirect.com

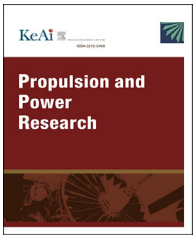

ORIGINAL ARTICLE

Deep learning-based modeling method for probabilistic LCF life prediction of turbine blisk

Cheng-Wei Fei[a], Yao-Jia Han[a], Jiong-Ran Wen[a], Chen Li[a], Lei Han[a], Yat-Sze Choy[b,*]

[a]*Department of Aeronautics and Astronautics, Fudan University, Shanghai 200433, China*
[b]*Department of Mechanical Engineering, Hong Kong Polytechnic University, Hong Kong 999077, China*

Received 8 February 2023; accepted 10 August 2023
Available online 12 October 2023

KEYWORDS

Convolutional-deep neural network;
Low cycle fatigue;
Life prediction;
Turbine blisk;
Probabilistic prediction

Abstract Turbine blisk is one of the typical components of gas turbine engines. The fatigue life of turbine blisk directly affects the reliability and safety of both turbine blisk and aeroengine whole-body. To monitor the performance degradation of an aeroengine, an efficient deep learning-based modeling method called convolutional-deep neural network (C-DNN) method is proposed by absorbing the advantages of both convolutional neural network (CNN) and deep neural network (DNN), to perform the probabilistic low cycle fatigue (LCF) life prediction of turbine blisk regarding uncertain influencing parameters. In the C-DNN method, the CNN method is used to extract the useful features of LCF life data by adopting two convolutional layers, to ensure the precision of C-DNN modeling. The two close-connected layers in DNN are employed for the regression modeling of aeroengine turbine blisk LCF life, to keep the accuracy of LCF life prediction. Through the probabilistic analysis of turbine blisk and the comparison of methods (ANN, CNN, DNN and C-DNN), it is revealed that the proposed C-DNN method is an effective mean for turbine blisk LCF life prediction and major factors affecting the LCF life were gained, and the method holds high efficiency and accuracy in regression modeling and simulations. This study provides a promising LCF life prediction method for complex structures, which contribute to monitor health status for aeroengines operation.

*Corresponding author.
E-mail address: yatsze.choy@polyu.edu.hk (Yat-Sze Choy).
Peer review under responsibility of Propulsion and Power Research.

ELSEVIER | Production and Hosting by Elsevier on behalf of KeAi

https://doi.org/10.1016/j.jppr.2023.08.005

1. Introduction

As the power source of airplanes, aeroengine is the important source of airplane faults, so that the reliability and safety of aeroengine are focused on recently [1]. As the key component of aeroengine, turbine blisk comprising disk and blades long-term works in extreme conditions with high temperature, high pressure, large stress, and high rotational speed, so that the safety and reliability of turbine blisk suffer from the serious challenge which severely affect the health status of aeroengines and airplanes [2]. Specially, such extreme conditions always result in the low cycle fatigue (LCF) of turbine blisk for long-term works, which have been attracting the attention of researchers, for ensuring the operation safety of aeroengine [3−5].

The LCF life prediction of turbine blisk involving disk and blades is one of significant topics in the health monitoring and safety operation of aeroengines, so that numerous prediction theory and methods emerged recently, such as neural network (NN) methods [6−9], Kriging models [10−12], support vector machine (SVM) methods [13−16], polynomials [17,18], and numerical methods [19−22]. Obviously, most of the mentioned works only focus on traditional numerical methods [23,24] and machine learning approaches [25]. Due to working in complex environments, naturally the LCF life prediction of turbine blisk holds high nonlinear and time-varying characteristics, due to large-scale operation parameters (hyperparameters) and transient loads, which lead to these methods to be unworkable in acquiring an acceptable modeling accuracy and computing efficiency in the LCF life prediction of turbine blisk [26−28]. Therefore, it is urgent to find new efficient manners with high precision and efficiency besides the skillful processing of hyperparameters and transients.

With the rapid development of structural LCF life prediction, deep learning as a new alternative technology have got widely studies and applications [29], so that various deep learning approaches also appeared [30−32]. Hereinto, convolutional neural network (CNN) and deep neural network (DNN) are two important types of deep learning algorithms. For the CNN, Yu et al. [33] discussed fault diagnosis of wind turbine systems by combining a spectrogram, and revealed the superior ability of CNN in feature extraction; Jiang et al. [34] studied the prediction of bearing remaining useful life by adopting time series multi-channel CNN with attention-based long short-term memory (LSTM) that's a type of DNN models; Zare and Ayati [35] investigated the simultaneous fault diagnosis of wind turbine using multichannel CNNs; Sony et al. [36], systematically reviewed structural condition assessment techniques based on CNN model; Wang et al. [37], applied simplified CNN to develop a light intelligent diagnosis model based on improved Online Dictionary Learning sample-making. These works revealed that the CNN method hold the capability of feature extraction in fault diagnosis. for the DNN, Kulkarni et al. [38], employed DNN to forecast wind speed for the fatigue analysis of a large composite wind turbine blade; Veloz et al. [39], utilized the DNN estimate the fatigue life of wind turbine blades from a probabilistic perspective; Xia et al. [40] employed the LSTM to estimate the remaining useful life of aeroengine during airplane flight with the combination with multi-layer self-attention method. The aforementioned works indicate that feature extraction and regression modeling are two key tasks which seriously influence the prediction precision of turbine blisk LCF life. Meanwhile, the CNN method presented excellent performance in feature extraction and the DNN method revealed unique superiority in parameters identification and regression modeling [41−43]. With the heuristic conclusions, it is promising to absorb the strengths of CNN and DNN in the LCF life prediction of turbine blisk. However, the previous works only depended on the single method such CNN method or DNN method. It is not found that the CNN method and DNN method were synthetically applied to improve the reasonability and effectiveness of structural probabilistic design by precisely feature identification and regression modeling.

In fact, the affecting parameters on the LCF life of turbine blisk have large uncertainty. To address this issue, many scholars investigated the LCF life prediction of turbine blisk from a probabilistic perspective [39,44−47]. Obviously, it is shown that probabilistic analysis can well handle the uncertainty of affecting parameters structural design, which provide a valuable idea for the LCF life of turbine blisk with uncertain factors. Therefore, it is urgent to find an efficient approach for the probabilistic LCF life of turbine blisk.

With the enlightenment of CNN, DNN and probabilistic approach in characteristics, the objective of this paper is to propose the convolutional-deep neural network (C-DNN) method, an efficient deep learning-based modeling method, by absorbing the advantages of CNN in feature extraction and DNN in regression modeling, to perform the probabilistic LCF life prediction of turbine blisk by fully respecting uncertain influencing parameters. In the developed C-DNN method, two convolutional layers in CNN method is adopted to extract the features of LCF life data, and two close-connected layers in DNN are employed for the regression modeling of aeroengine turbine blisk LCF life.

In what follows, Section 2 discusses the C-DNN method from three aspects, i.e., convolutional layer, maxpooling and flatten layer and closely-connected layer. The procedure and method for probabilistic LCF life prediction of turbine blisk with C-DNN are given in Section 3. In Section 4 the probabilistic LCF life prediction of turbine blisks is investigated in respect of the developed C-DNN method, involving the parameters selection and FE model of turbine blisk, the deterministic analysis of turbine blisk LCF life, the C-DNN modeling and validation for probabilistic blisk LCF life prediction, the probabilistic LCF life analyses of turbine blisk with C-DNN and comparison of methods. Main conclusions on this paper are summarized in Section 5.

2. Convolutional-based deep neural network methods

In this study, the C-DNN method is developed to perform the reliability sensitivity analyses of turbine blisk for predicting LCF life. The structure of the C-DNN method comprises convolutional layer, maxpooling and flatten layer and closely-connected layer, which are explained in Figure 1.

In Figure 1, maxpooling is pooling operation that calculates the maximum value for patches of a feature map, to create a downsampled (pooled) feature map. The maxpooling is usually used after convolutional layers. Flatten layer is used to flatten the inputs. For example, if flatten layer is applied to the input that is two-dimensional matrix, the output shape is a one-dimensional vector. In this section, the operations of convolutional layer in CNN and closely-connected layer in DNN is discussed in the following subsections.

2.1. Convolutional neural network

In CNN method, convolutional layer is the first layer to extract the features from an input vector that comprises input parameters. Convolution is the operation of a vector and a filter or kernel. For one-dimensional (1-D) CNN, the operation with input parameters, Kernel and output parameters is illustrated in Figure 2.

In Figure 2, $\boldsymbol{x}=(x_1, x_2, \cdots, x_i, \cdots, x_n)$ is the vector of input parameters in which x_i indicates ith element and n is the length of input parameters in the vector. s stands for the stride which is the number of pixels shifts over the input vector. $\boldsymbol{z}=(z_1, z_2, \cdots, z_j, \cdots, z_k)$ is the vector of filter

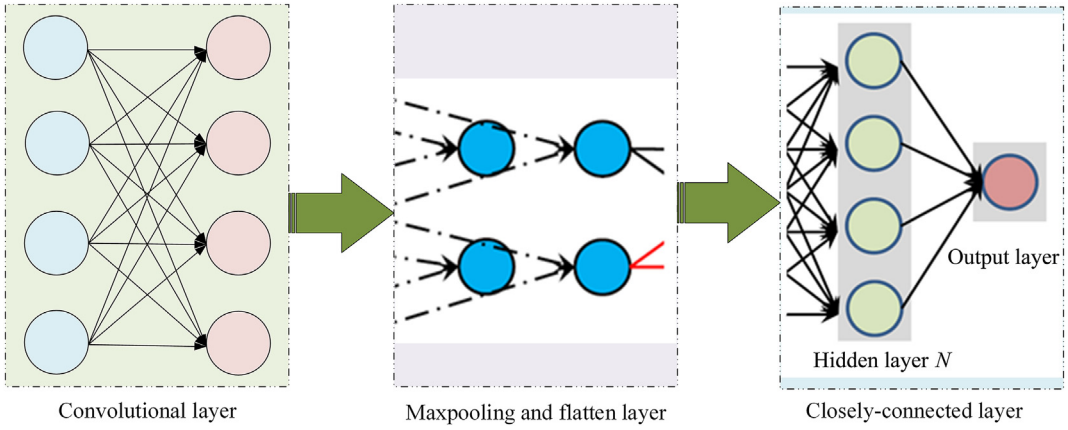

Figure 1 Structure of convolutional-based deep neural network.

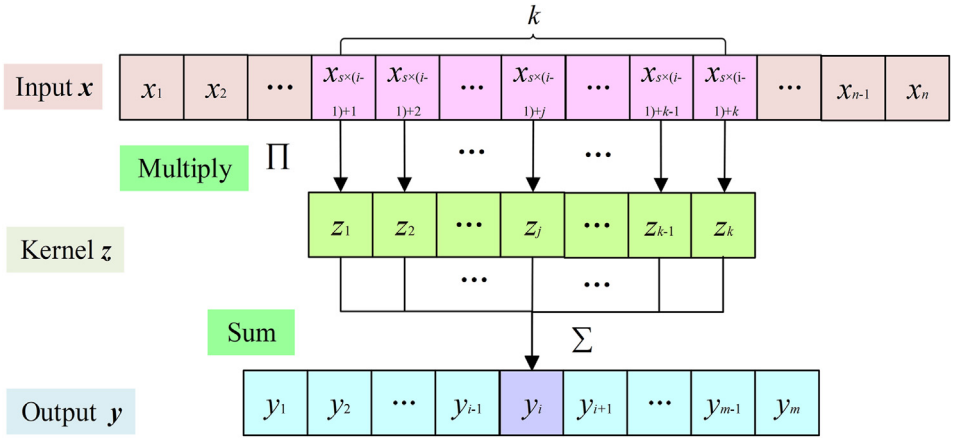

Figure 2 Principle of 1D convolutional layer.

composed by k elements in $\boldsymbol{z}$, in which the subscript j indicates the jth element in the vector $\boldsymbol{z}$ and k is the length of the filter vector; $\boldsymbol{y}=(y_1, y_2, \cdots, y_i, \cdots, y_m)$ is the vector of output parameters where y_i represents the ith element and m represents the length of output vector.

Considering the explanation in Figure 2, the relationship among the length n of input vector $\boldsymbol{x}$, the length m of output vector $\boldsymbol{y}$ and the length k of filter vector $\boldsymbol{z}$ are

$$m = \frac{n-k}{s} \tag{1}$$

Stride is the number of pixels shifting over the input vector. When the strides are 1, the filter moves one step at a time, while the filter moves two steps at a time when the stride is 2, in a similar fashion. However, when $\frac{n-k}{s}$ is not an integer, the padding method [36] is used to update the length n of input vector, including two methods. One is that zero is applied to fill the vector of input vector (called as zero-padding), to adapt the filter. The other is that the improper part in input vector is deleted by and only remaining the effective part of input vector, which is called valid padding method.

In line with the 1-D convolutional calculation, the ith output response y_i is

$$y_i = \sum_{j=1}^{k} z_j x_{s\times(i-1)+j} \tag{2}$$

In fact, this study applies many filters, the number n_p of weight parameters is

$$n_p = k \times D_{input} \times D_{output} \tag{3}$$

where D_{input} is the number of filters of the previous 1-D convolutional layer; D_{output} is the number of filters in the 1-D convolutional network of this convolutional layer.

The number of output parameters in the 1-D CNN is

$$V_{output} = m \times D_{output} \tag{4}$$

where V_{output} is the number of output parameters.

2.2. Deep neural network

Deep neural network is one branch of deep learning method [39], in which the "deep" indicates many layers. It is obvious that deep neural network involves multiple layers of neural networks. The features of data are passed to the model, and then neural network attempts to represent the data in different ways and in different dimensions by applying specific operations. On a lower level, neural networks are a combination of elementary operations on matrices and nonlinear functions as illustrated in Figure 3.

In Figure 3, the circles are a neuron and the arrows are to connect neurons by close connections. The output of a neuron is determined by the output of neuron in previous layer, the corresponding weight and the bias, which is expressed by

$$p = \left(\sum_{r=0}^{a} w_r t_r\right) + \theta \tag{5}$$

in which w is the weight of each neuron connection; t denotes the output of previous neuron; θ indicates the deviation of the current neuron and is a constant; a is the number of neurons connections between input layer and first hidden layer; p is the output of neuron in output layer; r indicates the rth neuron connection between input layer and first hidden layer.

To model high-dimensional data, an activation function $F(\cdot)$ is adopted to increase the complexity and dimension of the network, i.e.,

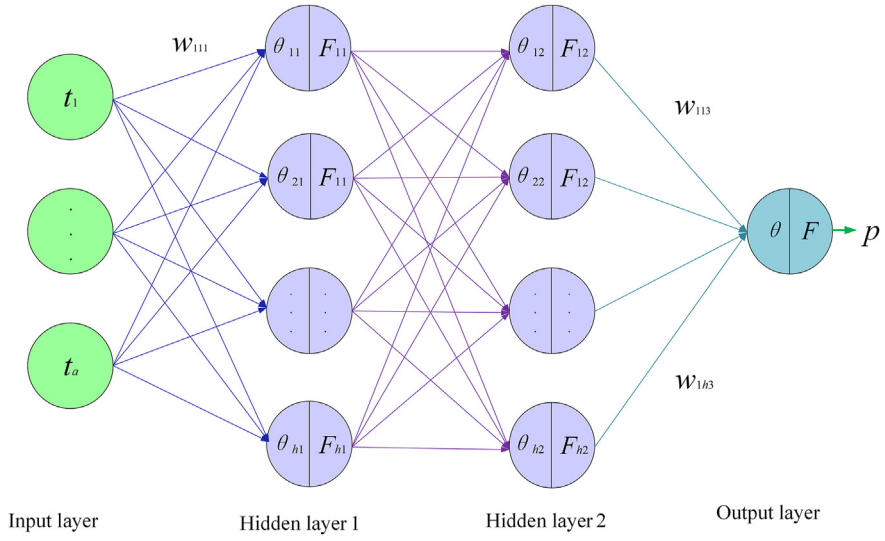

Figure 3 Principle of deep neural network.

$$p = F\left(\left(\sum_{r=0}^{a} w_r t_r\right) + \theta\right) \tag{6}$$

3. Procedure and method for probabilistic LCF life prediction of turbine blisk with C-DNN

3.1. Probabilistic LCF life prediction flowchart of turbine blisk

In light of the introduced theory and methods, the probabilistic LCF life prediction flowchart of turbine blisk with C-DNN method is summarized as follows.

Step 1: Take the temperature, speed, material properties and LCF performance parameters of turbine blisk as input random variables to establish the finite element (FE) model of turbine blisk.

Step 2: Perform deterministic FE analysis of turbine blisk to obtain the position of the minimum fatigue life of the blisk as the calculation point in respect of thermo-structure coupling and boundary conditions.

Step 3: Apply Latin hypercube sampling (LHS) method [12] to extract small batches of samples for input random variables, and the gain the corresponding output samples of blisk LCF life by blisk FE analyses for all input samples at the calculation point.

Step 4: Divide the samples involving all input samples and their corresponding output samples into training samples set and test samples set.

Step 5: Normalize all samples and adjust learning rate,

Step 6: Select a part of the samples as the training samples to establish the C-DNN model of probabilistic LCF life of turbine blisk.

Step 7: Regard the remaining samples as the test samples to check if the accuracy of the established C-DNN model is larger than 0.95. If it does not meet, go back to **Step 3**; if it meets, go to **Step 8**.

Step 8: Output the parameters of C-DNN model, including weights, biases, learning rate, and so forth, to determine the C-DNN model for the probabilistic LCF life prediction of turbine blisk.

Step 9: Perform the probabilistic LCF life prediction of turbine blisk, involving sensitivity analysis and reliability analysis, by employing Monte Carlo (MC) method [27] to simulate large-scale samples for both input random variables and output variable respecting the built C-DNN model, which follow the distribution features of input and output parameters.

Step 10: Output the results of sensitivity analysis and reliability analysis, and then end the task.

As illustrated in the above analysis, the LCF life reliability analyses of turbine blisk with C-DNN method many involve LCF life analysis with FE model, C-DNN modeling for probabilistic LCF life and probabilistic LCF life analysis. The process of turbine blisk LCF life prediction with C-DNN is shown in Figure 4.

3.2. Reliability sensitivity calculation method

Assuming y^* is the allowable value of low-cycle fatigue life and $y^j_{\min}$ is the function of structural fatigue life, the limit state function of the low-cycle fatigue life of structure [47] is:

$$Z = y_{\min} - y^* \tag{7}$$

When the limit state function $Z > 0$ means that the actual minimum fatigue life of the blisk is greater than the allowable value, so that the blisk structure is safe; otherwise, the structure fails [46]. Assuming that the input random variables in Eq. (7) are independent from each other, the mean and variance matrices are $\boldsymbol{\mu} = [\mu_1, \mu_2, \cdots, \mu_n]$ and $\boldsymbol{D} = [D_1, D_2, \cdots, D_n]$, then

$$\begin{cases} E(Z) = \boldsymbol{\mu}_Z(\mu_1, \mu_2, \cdots, \mu_n; D_1, D_2, \cdots, D_n) \\ D(Z) = \boldsymbol{D}_Z(\mu_1, \mu_2, \cdots, \mu_n; D_1, D_2, \cdots, D_n) \end{cases} \tag{8}$$

in which $E(Z)$ is the mean function; $D(Z)$ is the variance function.

When the low fatigue cycle limit equation of the structure obeys a normal distribution, the reliability of structure [8,9] can be expressed as

$$P_r = \phi\left(\frac{\boldsymbol{\mu}_Z}{\sqrt{\boldsymbol{D}_Z}}\right) \tag{9}$$

in which P_r is the probability that the structure can complete its predetermined function; $\boldsymbol{\mu}_Z$ is the mean matrix of the limit state function; $\boldsymbol{D}_Z$ is the variance matrix of the limit state function.

Sensitivity reflects the sensitivity degree of input random variable to the failure probability of structural system response, so as to determine which input random variable are larger influencing factors to provide guidance for structural optimization. The sensitivity of reliability to the mean matrix $\boldsymbol{\mu}$ and variance matrix $\boldsymbol{D}$ of input random variables [12] is expressed as

$$\begin{cases} \dfrac{\partial P_r}{\partial \boldsymbol{\mu}^{\mathrm{T}}} = \dfrac{\partial P_r}{\partial\left(\dfrac{\boldsymbol{\mu}_Z}{\sqrt{\boldsymbol{D}_Z}}\right)}\left(\dfrac{\partial\left(\dfrac{\boldsymbol{\mu}_Z}{\sqrt{\boldsymbol{D}_Z}}\right)}{\partial \boldsymbol{\mu}_Z}\dfrac{\partial \boldsymbol{\mu}_Z}{\partial \boldsymbol{\mu}^{\mathrm{T}}} + \dfrac{\partial\left(\dfrac{\boldsymbol{\mu}_Z}{\sqrt{\boldsymbol{D}_Z}}\right)}{\partial \boldsymbol{D}_Z}\dfrac{\partial \boldsymbol{\mu}_Z}{\partial \boldsymbol{\mu}^{\mathrm{T}}}\right) \\ \dfrac{\partial P_r}{\partial \boldsymbol{D}^{\mathrm{T}}} = \dfrac{\partial P_r}{\partial\left(\dfrac{\boldsymbol{\mu}_Z}{\sqrt{\boldsymbol{D}_Z}}\right)}\left(\dfrac{\partial\left(\dfrac{\boldsymbol{\mu}_Z}{\sqrt{\boldsymbol{D}_Z}}\right)}{\partial \boldsymbol{\mu}_Z}\dfrac{\partial \boldsymbol{\mu}_Z}{\partial \boldsymbol{D}^{\mathrm{T}}} + \dfrac{\partial\left(\dfrac{\boldsymbol{\mu}_Z}{\sqrt{\boldsymbol{D}_Z}}\right)}{\partial \boldsymbol{D}_Z}\dfrac{\partial \boldsymbol{\mu}_Z}{\partial \boldsymbol{D}^{\mathrm{T}}}\right) \end{cases} \tag{10}$$

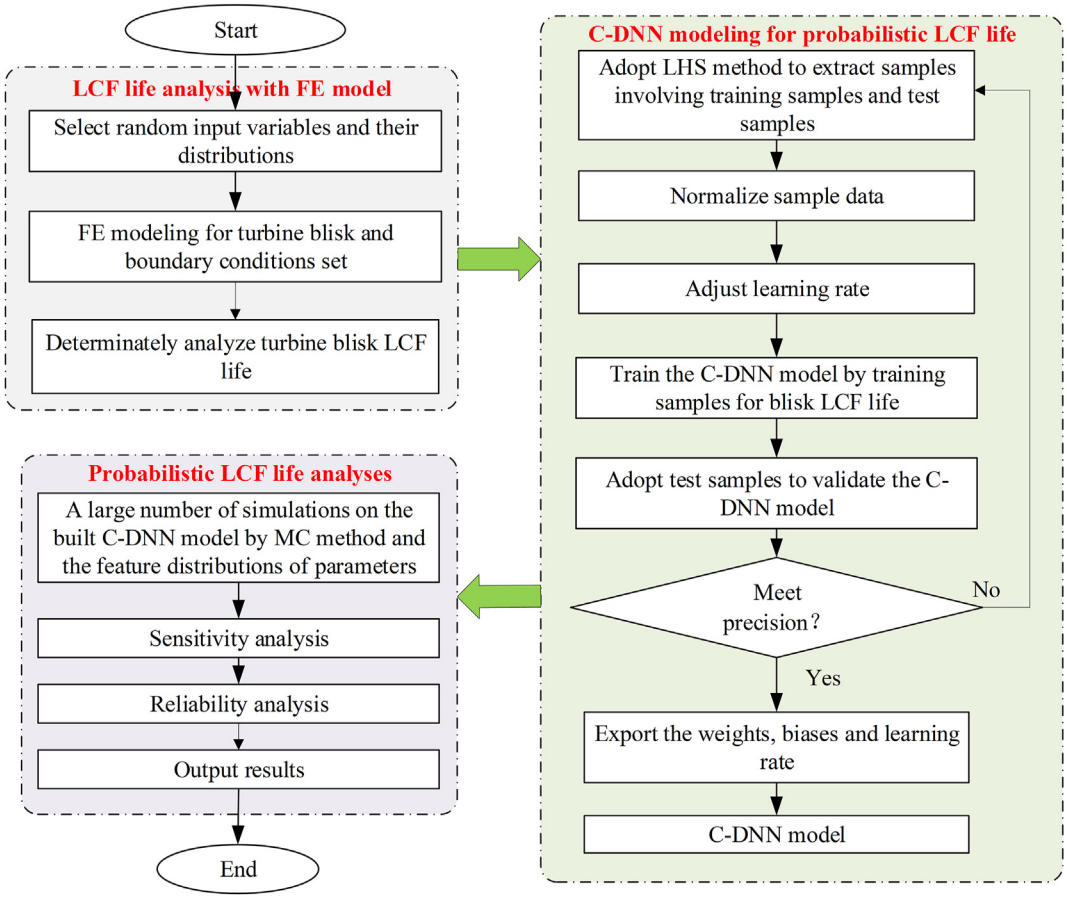

Figure 4 Flowchart of LCF life prediction of turbine blisk with C-DNN method.

$$\begin{cases} \dfrac{\partial P_r}{\partial\left(\dfrac{\boldsymbol{\mu}_Z}{\sqrt{\boldsymbol{D}_Z}}\right)}=\phi\left(\dfrac{\boldsymbol{\mu}_Z}{\sqrt{\boldsymbol{D}_Z}}\right);\ \dfrac{\partial\left(\dfrac{\boldsymbol{\mu}_Z}{\sqrt{\boldsymbol{D}_Z}}\right)}{\partial\boldsymbol{\mu}_Z}=\dfrac{1}{\sqrt{\boldsymbol{D}_Z}};\ \dfrac{\partial\left(\dfrac{\boldsymbol{\mu}_Z}{\sqrt{\boldsymbol{D}_Z}}\right)}{\partial\boldsymbol{D}_Z}=-\dfrac{\boldsymbol{\mu}_Z}{2}\boldsymbol{D}_Z^{-\frac{3}{2}} \\ \dfrac{\partial\boldsymbol{\mu}_Z}{\partial\boldsymbol{\mu}^{\mathrm{T}}}=\left[\dfrac{\partial\boldsymbol{\mu}_Z}{\partial\mu_1},\dfrac{\partial\boldsymbol{\mu}_Z}{\partial\mu_2},\cdots,\dfrac{\partial\boldsymbol{\mu}_Z}{\partial\mu_n}\right]^{\mathrm{T}};\ \dfrac{\partial\boldsymbol{\mu}_Z}{\partial\boldsymbol{D}^{\mathrm{T}}}=\left[\dfrac{\partial\boldsymbol{\mu}_Z}{\partial D_1},\dfrac{\partial\boldsymbol{\mu}_Z}{\partial D_2},\cdots,\dfrac{\partial\boldsymbol{\mu}_Z}{\partial D_n}\right]^{\mathrm{T}} \\ \dfrac{\partial\boldsymbol{D}_Z}{\partial\boldsymbol{\mu}^{\mathrm{T}}}=\left[\dfrac{\partial\boldsymbol{D}_Z}{\partial\mu_1},\dfrac{\partial\boldsymbol{D}_Z}{\partial\mu_2},\cdots,\dfrac{\partial\boldsymbol{D}_Z}{\partial\mu_n}\right]^{\mathrm{T}};\ \dfrac{\partial\boldsymbol{D}_Z}{\partial\boldsymbol{D}^{\mathrm{T}}}=\left[\dfrac{\partial\boldsymbol{D}_Z}{\partial D_1},\dfrac{\partial\boldsymbol{D}_Z}{\partial D_2},\cdots,\dfrac{\partial\boldsymbol{D}_Z}{\partial D_n}\right]^{\mathrm{T}} \end{cases} \tag{11}$$

4. Probabilistic LCF life prediction of turbine blisks

4.1. Parameters selection and FE model

This section selects the turbine blisk of aeroengine as the object of study. The materials of turbine blisk is GH4133 superalloy [48]. For the low-cycle fatigue life reliability analysis of the blisk, the influencing factors include numerous parameters and hold uncertainty, involving operation parameters (temperature T and rotational speed ω) and material parameters such as density ρ, thermal conductivity λ and elastic modulus E, fatigue strength coefficient σ_f', fatigue ductility coefficient ε_f', fatigue strength index b and fatigue ductility index c. In respect of the Manson-Coffin raw [49,50], the relationship among fatigue strength coefficient σ_f', fatigue ductility coefficient ε_f', fatigue strength index b and fatigue ductility index c are expressed by:

$$\frac{\Delta\varepsilon}{2}=\frac{\sigma_f'}{E}(2N_f)^b+\varepsilon_f'(2N_f)^c \tag{12}$$

in which $\Delta\varepsilon$ is the total strain; N_f is the LCF of turbine blisk [9].

Regarding complex workloads and the influence of the average stress, Eq. (12) can be rewritten as [49].

$$\frac{\Delta\varepsilon}{2}=\frac{\sigma_f'-\sigma_m}{E}(2N_f)^b+\varepsilon_f'(2N_f)^c \tag{13}$$

where σ_m is average stress.

To support the analysis with less computational load and small complication, the aforesaid random variables are assumed to be independent mutually and obey normal distributions. Their distribution features are assumed as shown in Table 1.

In the LCF life analysis of turbine blisk, 1/40 turbine blisk comprising 1/40 disk and one blade is regarded to reduce the computational loads, because the selected blisk as an axisymmetric structure is composed by one disk and 40 blades. In the used FE model of blisk, there are 31,380 nodes and 17,111 tetrahedral elements. The 1/40 turbine blisk is built as FE model and is meshed with tetrahedral elements.

4.2. Deterministic analysis of turbine blisk LCF life

Due to the small influence of aerodynamic loads on turbine blisk LCF life relative to centrifugal load and thermal load, thermal-solid interaction [51,52] is employed in the deterministic analysis of turbine blisk in Ansys program without aerodynamic effect, by considering the uncertain parameters in Table 1. Through the analysis, the maximum equivalent stress and equivalent strain of the blisk are located at the root of the blade, and the maximum stress is 105.77 MPa, and the maximum strain is 8.1427×10^{-3} m/m. For this reason, the maximum strain point of the blade root was selected for the LCF life analysis of turbine blisk. The deterministic analysis of turbine blisk LCF life is to comprehensively consider the influence of structural stress and strain on the structural durability. According to Eq. (12) and Eq. (13), the fatigue life of the blisk is calculated as displayed in Figure 5, indicating that the minimum blisk life is 8900.6 cycles.

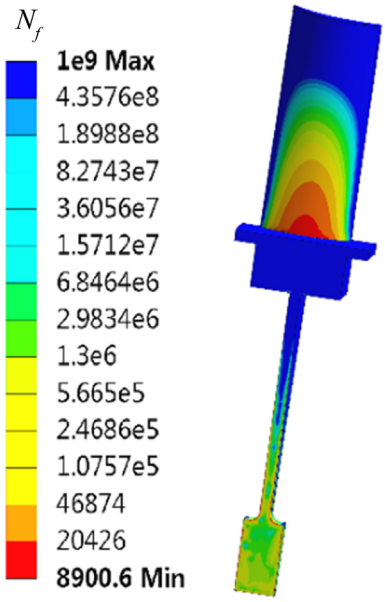

Figure 5 Nephograms of blisk LCF life distribution.

4.3. C-DNN modeling and validation for probabilistic blisk LCF life prediction

In line with the distributions of input random variables in Table 1, the LHS method is adopted to extract 1000 samples by FE analyses. To more reasonably use the samples, the extracted samples of input variables are normalized in light of Eq. (14) [10]. After normalization processing, the distribution features of *i*th input variables are acquired in Table 2.

$$x_i'=\frac{x_i-\min(\boldsymbol{X})}{\max(\boldsymbol{X})-\min(\boldsymbol{X})} \tag{14}$$

where x_i is the *i*th element in input variable vector $\boldsymbol{x}=(x_1, x_2,\cdots,x_k)$; x_i' indicates the *i*th element in the initialized input variable vector $\boldsymbol{x}'=(x_1',x_2',\cdots,x_k')$; k is the number of input variables; min($\boldsymbol{X}$) represents the smallest element in $\boldsymbol{X}$; max($\boldsymbol{X}$) denotes the largest element in $\boldsymbol{X}$.

Table 1 The distribution features of selected random variables.

Parameters	Mean	Standard deviation	Minimum	Maximum	Count
Density ρ (kg·m^{-3})	8213.5758	735.9972	6949.9166	9470.0834	150
Rotating speed ω (rad·s^{-1})	1169.0416	104.1095	988.7336	1347.2664	150
High temperature magnitude T_b (K)	1471.5031	130.9990	1246.9217	1699.0783	150
Low temperature magnitude T_a (K)	1173.9488	104.6953	992.9662	1353.0338	150
Elastic modulus E (GPa)	216.9535	19.4795	183.6945	250.3055	150
Thermal conductivity λ (W·m^{-1}·C^{-1})	21.8868	1.9601	18.5388	25.2612	150
Fatigue strength index b	−0.1001	0.0089	−0.1153	−0.0847	150
Fatigue ductility index c	−0.8394	0.0751	−0.9689	−0.7111	150
Fatigue strength coefficient σ'_f	1419.0687	127.4320	1201.2097	1636.7903	150
Fatigue ductility coefficient ε'_f	50.5094	4.5337	42.7492	58.2508	150

Table 2 Normalized distribution features of random variables.

Parameters	Mean	Standard deviation	Minimum	Maximum	Count
Density ρ ($kg \cdot m^{-3}$)	0.5014	0.2920	0.0	1.0	150
Rotating speed ω ($rad \cdot s^{-1}$)	0.5029	0.2904	0.0	1.0	150
High temperature magnitude T_b (K)	0.4967	0.2897	0.0	1.0	150
Low temperature magnitude T_a (K)	0.5026	0.2908	0.0	1.0	150
Elastic modulus E (GPa)	0.4993	0.2924	0.0	1.0	150
Thermal conductivity λ ($W \cdot m^{-1} \cdot C^{-1}$)	0.4980	0.2916	0.0	1.0	150
Fatigue strength index b	0.4978	0.2913	0.0	1.0	150
Fatigue ductility index c	0.5023	0.2912	0.0	1.0	150
Fatigue strength coefficient σ'_f	0.5014	0.2920	0.0	1.0	150
Fatigue ductility coefficient ε'_f	50.5094	4.5337	42.7492	58.2508	150

The acquired 1000 samples are divided into two sets involving 800 samples and 200 samples. The 800 samples are selected as the training samples for C-DNN modeling, and the remaining 200 samples as the test samples are employed to test the built C-DNN model. In the C-DNN model, an eight-layer network with a total of 6779 parameters are elected including input layer (10 neurons), two convolutional layers (the sizes of filters are 5 and 10, respectively), maxpooling layer (the size of filter is 3), flatten layer (to make the output of the maxpooling layer into a one-dimensional vector), two close-connected layers with 64 neurons for one layer, and output layer with one neuron.

After training C-DNN model, the rest 200 samples are applied to test the built C-DNN model. Here, the mean absolute error (MAE) and mean square error (MSE) are adopted to reflect the effect of C-DNN modeling. The MAE and MSE are expressed by

$$MSE = \sqrt{\frac{\sum_{i=1}^{n} (p_i - Y_i)^2}{n}} \tag{15}$$

$$MRE = \sqrt{\frac{\sum_{i=1}^{n} |p_i - Y_i|}{n \times Y}} \tag{16}$$

where p_i is the predicted value of ith sample; Y_i is the real value of ith sample; n indicates the number of samples.

The historical processes of MAE and MSE for training samples and test samples are generated as shown in Figure 6, in which the blue line stands for training samples set and the orange line indicates test sample set.

As illustrated in Figure 6, in the training progress, the MAE and MSE values of test set and training set decrease. The MAE of test set is used as monitoring the training.

By inputting the test set of 200 samples into the built C-DNN model, the prediction values of blisk LCF life are gained to compare with the true values. The comparison results are listed in Table 3.

As seen in Table 3, the predicted value is very close to the true value. To observe the difference between the predicted value and the true value, the scatter diagram is shown in Figure 7.

As seen in Figure 7, the points above the middle line mean that predicted values are bigger than true value. When the points below the middle line indicate that the true values are bigger than the predicted values. No matter what range of the output value is, the predicted value is very close to the true value.

4.4. LCF life reliability evaluation of turbine blisk with C-DNN model

10,000 samples are extracted to and inputted into the built C-DNN model to get the corresponding predicted

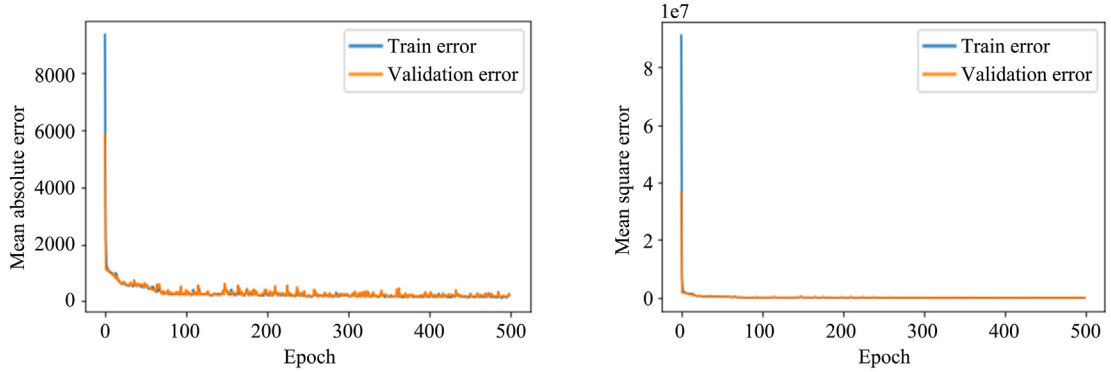

(a) Mean ABS errors (b) Mean square errors

Figure 6 Pressure history of six-tube working together within 20 s.

Table 3 The comparison results of true values and predictions.

Sample index	True values, cycles	Predictions, cycles
545	10824.3101	10813.6885
298	9076.1018	9468.6143
109	7643.5650	7535.0151
837	12058.8043	11959.6807
194	8959.1333	9239.8027
…	…	…
68	13040.5261	12818.1152
449	9129.2682	9180.2725
715	7494.8473	7428.8262
793	10866.3081	10993.2236
688	9371.1422	9462.5518

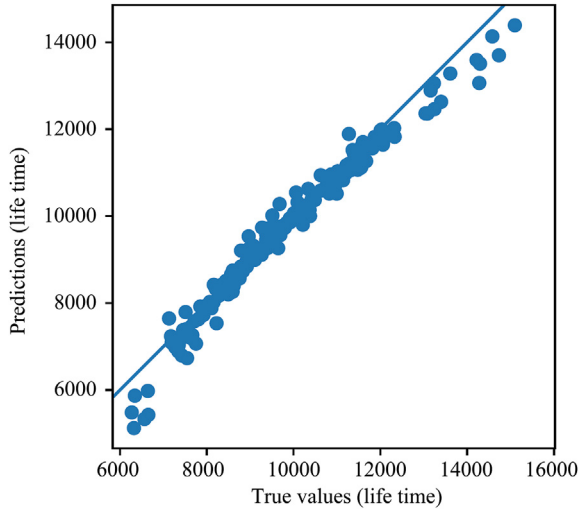

Figure 7 The scatter diagram of true values and prediction values.

values $\{y_{\min}\}$ according to Eqs. (7)−(9). The reliability of blisk LCF life with C-DNN model are obtained in different life allowable values and is listed in Table 4.

As shown in Table 4, the reliability R is about 0.996 when the confidence interval is 0.99 and the allowable LCF value is 5300 cycles. Therefore, the allowable LCF life of turbine blisk should be 5300 cycles with regard to the safety and reliability of the turbine blisk.

4.5. Probabilistic LCF life analyses of turbine blisk with C-DNN

100,000 simulations for the C-DNN model are performed by adopting MC method, and Eqs. (7)−(11) are applied to calculate the sensitivity degrees of random variables on turbine blisk LCF life as shown in Table 5 and Figure 8.

As demonstrated in Table 5 and Figure 8, the sensitivity of variables can be distinguished by the symbols "-" and "+", in which the symbol "-" indicate that the input variables negatively correlate with the blisk LCF life, such as rotational speed ω, and vice versa. Besides, the fatigue ductility index c is the main factor of affecting the blisk LCF life and its influence probability is about 28%. In this case, it

Table 4 Reliability degrees under different LCF allowable values.

LCF allowable value, cycles	Reliability degrees
2300	0.9999958
3300	0.9999448
4300	0.9994783
5300	0.9964324
6300	0.9822391
7300	0.9350194

Table 5 Sensitivity and impact ratio of random variables.

Random variables	Sensitivity degrees	Impact ratio (%)
Density ρ (kg·m^{-3})	0.0558	2.2776
Rotating speed ω (rad·s^{-1})	−0.1135	4.6311
High temperature magnitude T_b (K)	0.1535	6.2648
Low temperature magnitude T_a (K)	0.0894	3.6466
Elastic modulus E (GPa)	−0.0005	0.0214
Thermal conductivity λ (W·m^{-1}·C^{-1})	0.2583	10.539
Fatigue strength index b	0.3414	13.920
Fatigue ductility index c	0.675	27.546
Fatigue strength coefficient σ'_f	0.408	16.6579
Fatigue ductility coefficient ε'_f	0.355	14.4921

is deduced that the fatigue ductility coefficient c has the greatest impact on the reliability of turbine blisk LCF life, and then the fatigue strength index b, fatigue strength coefficient σ'_f, thermal conductivity λ, gas temperature T, rotational speed ω, density ρ and elastic modulus E are ordered by importance. The conclusions can provide a promising guidance for the optimization design of turbine blisk in advanced aeroengine development.

4.6. Comparison of methods

4.6.1. Accuracy validation in modeling and prediction

To highlight the strengths of the developed C-DNN method, the C-DNN method is compared to other methods involving ANN method, CNN method and DNN method by the reliability modeling and reliability prediction of turbine blisk LCF life. From the study, the MREs between the predicted values and the true values for the four methods are shown in Table 6, which are visualized in Figures 9−12.

As seen from Figures 9−12 and Table 6, from the perspective of reliability modeling accuracy, the MRE and accuracy of ANN modeling is 0.1233 and 0.8767, respectively, based on 800 modeling samples, while all the modeling accuracies of CNN, DNN and C-DNN are larger than 0.91. Especially, the modeling accuracy of C-DNN reaches to 0.9829, which is improved by ~6% compared with the CNN and DNN methods, and 10.62% compared with the traditional ANN, which is more than 10%. Therefore, the C-DNN method has high modeling accuracy. In addition, it can be seen from Table 6 that the C-DNN model firstly adopts two

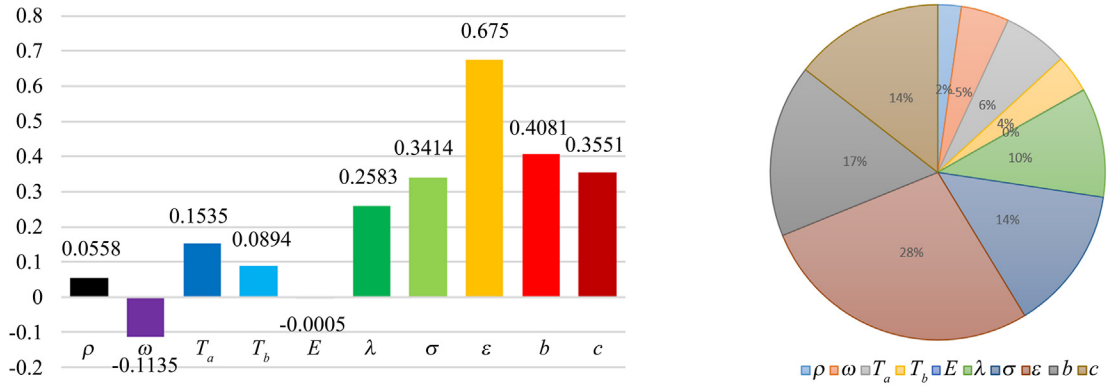

(a) Sensitivity histogram (b) Effect probability

Figure 8 Distributions of input variables to turbine blisk LCF life.

Table 6 The MREs of 200 samples.

models	Reliability modeling			Model-based reliability prediction		
	Number of training samples	MRE	Accuracy	Number of test samples	MRE	Accuracy
ANN	800	0.1233	0.8767	200	0.1431	0.8569
CNN		0.0816	0.9184		0.0924	0.9076
DNN		0.0772	0.9228		0.0861	0.9139
C-DNN		0.0171	0.9829		0.0237	0.9763

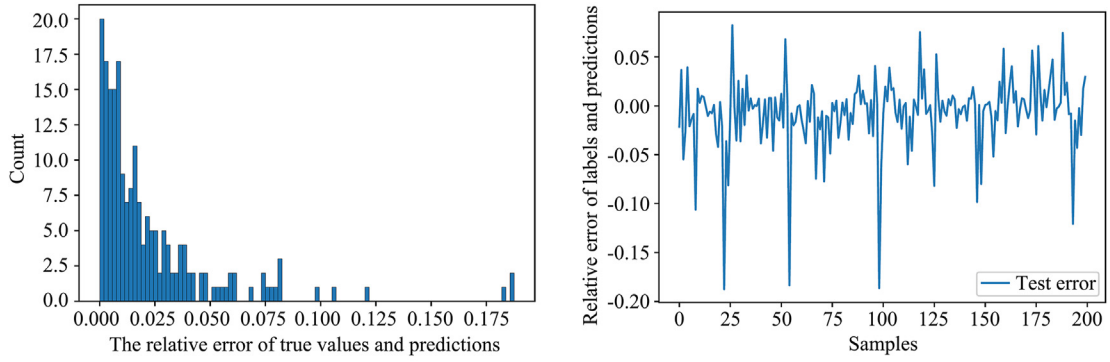

(a) Histogram (b) Historical curve

Figure 9 Relative errors between ANN prediction values and true values.

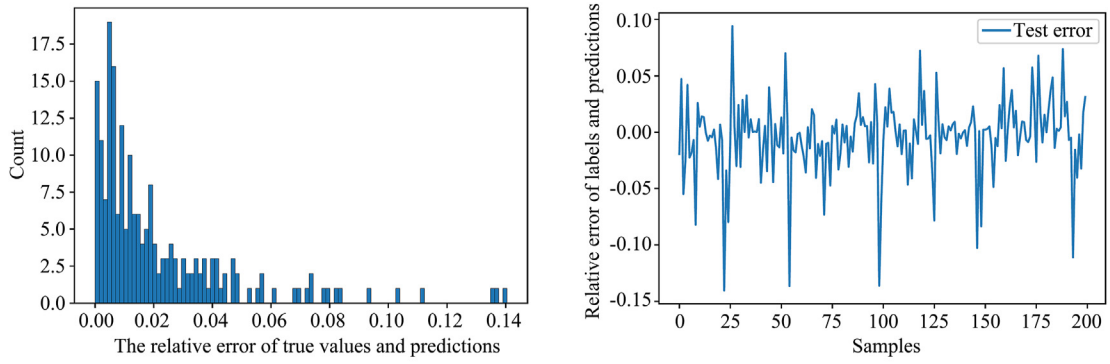

(a) Histogram (b) Historical curve

Figure 10 Relative errors between CNN prediction values and true values.

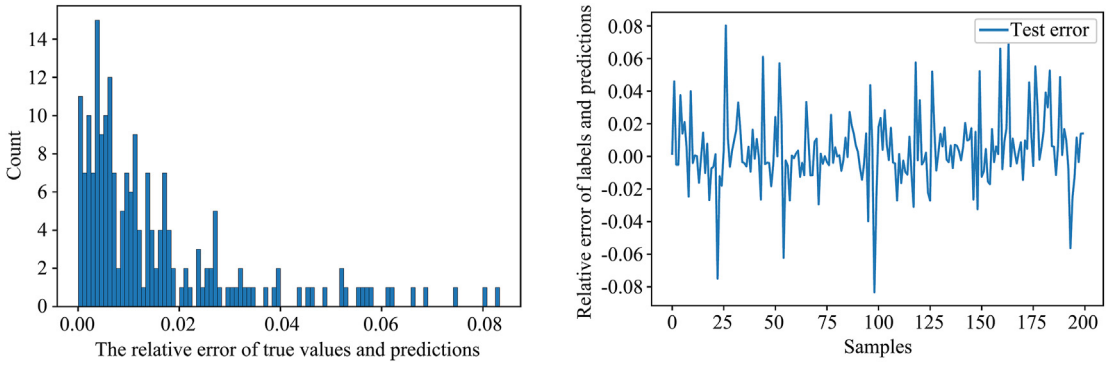

(a) Histogram (b) Historical curve

Figure 11 Relative errors between DNN prediction values and true values.

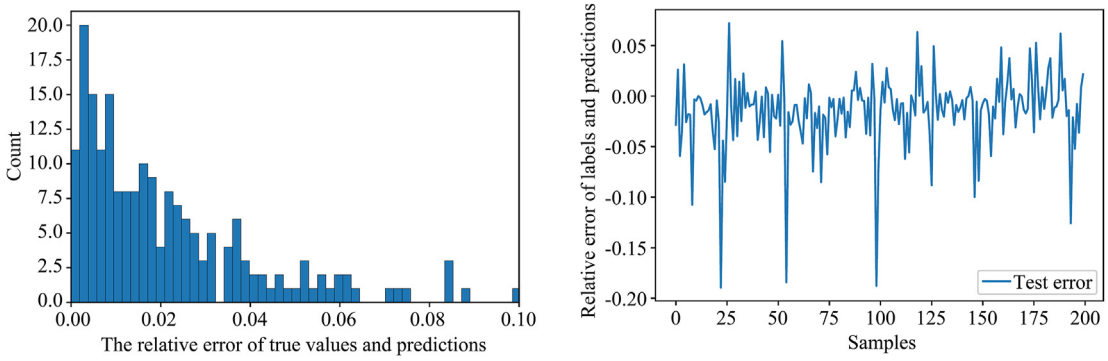

(a) Histogram (b) Historical curve

Figure 12 Relative errors between C-DNN prediction values and true values.

convolutional layers and two dense connection layers. After extracting the features of the data and then analyzing the connections between the simplified input parameters, the average relative error obtained is smaller than these obtained by using CNN method or DNN method alone.

From the perspective of reliability prediction accuracy, the reliability prediction evaluation accuracy of C-DNN model is 0.9763 and over 90%, which is improved by 6%–12% compared with the other three methods (ANN, CNN and DNN), especially by ~12% compared with the traditional ANN method. It is verified that the C-DNN method proposed in this study has high reliability prediction accuracy, strong learning ability and good generalization ability.

To demonstrate the prediction performance of C-DNN method, the C-DNN model are conducted by 10,000 simulations to predict the LCF life $y_{\min}$ of turbine blisk. Simultaneously, the built CNN model and DNN model are also performed for 10,000 simulations. In light of Eqs. (7)–(9), then the reliability degrees of blisk LCF life with the three methods can be acquired as shown in Table 7.

As illustrated in Table 7, the reliability degrees predicted by the C-DNN model is slightly lower than these of CNN model and DNN model, it is indicated that the developed C-DNN method are superior to the rest two methods CNN and DNN for the reliability prediction of turbine blisk LCF life, which is beneficial to improve the safety and reliability of engineering structures by focusing on structural strength.

4.6.2. Efficiency validation in modeling and prediction

To highlight the strengths of the proposed C-DNN method in modeling, 800 samples is utilized to build the models of four machine learning methods (ANN, CNN, DNN and C-DNN). The modeling time is shown in Table 8.

As illustrated in Table 8, among the four methods, the ANN method has the shortest modeling time 18.7624 s, and the C-DNN method is the longest modeling time 33.6986 s. Because the ANN method only involves hidden layers and few model parameters, so that in the process of parameter optimization, the ANN method has a smaller number of iterations, and spend less time and high modeling efficiency. However, CNN, and DNN within C-DNN belongs to the deep neural network, which involve multiple hidden layers, more parameters to optimize, more time spent, and low modeling efficiency. However, although the modeling time of C-DNN is longer than other methods, its modeling time is acceptable in terms of engineering.

Table 7 Comparisons of blisk LCF life reliability analyses with three methods.

Allowance value	Reliability degree			
	ANN	CNN	DNN	C-DNN
2300	0.9999960	0.9999995	0.9999972	0.9999958
3300	0.9999478	0.9999897	0.9999605	0.9999448
4300	0.9995035	0.9998468	0.9996054	0.9994783
5300	0.9965839	0.9984681	0.9971572	0.9964324
6300	0.9828826	0.9896314	0.9851563	0.9822391
7300	0.9369518	0.9519648	0.9432992	0.9350194

Table 8 Modeling time for four methods.

Methods	Modeling time
ANN	18.7624 s
CNN	32.4134 s
DNN	21.9149 s
C-DNN	33.6986 s

Table 9 Simulation time of four methods.

Iterations, times	C-DNN	CNN	DNN	ANN
5000	8.6019 s	9.5483 s	8.2398 s	7.7197 s
10,000	20.1177 s	28.7116 s	24.6505 s	25.3965 s
50,000	32.6009 s	37.99 s	35.9989 s	34.3695 s

In order to verify the simulation efficiency of C-DNN method, 5000 simulations, 10,000 simulations and 50,000 simulations were conducted by the built models, respectively. The simulation time of the four methods is shown in Table 9.

As shown in Table 9, the C-DNN has the shortest running time, with 8.6019 s for 5000 simulations, 20.1177 s for 10,000 simulations and 32.6009 s for 50,000 simulations. For 10,000 simulations, compared with the simulation time 25.3965 s of the traditional ANN model, the simulation time of the proposed C-DNN method is 20.1177 s, which is reduced by ∼5 s, and improves the simulation efficiency by ∼20%. Therefore, the proposed C-DNN method is demonstrated to be high efficiency in modeling and reliability prediction and is a promising approach for the probabilistic LCF life design of complex structures besides turbine blisk.

5. Conclusions

This study proposes a novel prediction method, convolutional-deep neural network (C-DNN), and performs the reliability modeling and evaluation of turbine blisk low cycle fatigue (LCF) life. Through the detailed investigation, main conclusions are summarized as follows.

(1) CNN can effectively extract the features of samples in the LCF life modeling of turbine blisk.
(2) DNN has better abilities in parameters identification and regression modeling for the LCF life prediction of turbine blisk.
(3) The consideration of the uncertainty of affect parameters can improve the estimation accuracy and modeling precision, which enhance the LCF life prediction of turbine blisk.
(4) Fatigue ductility index with the influence ratio 28% is the major factor and is positively correlated with the LCF of turbine blisk.
(5) The proposed C-DNN model has high modeling accuracy and test accuracy for good learning ability, generalization ability, strong robustness and good prediction effect in the LCF life valuation of turbine blisk.
(6) C-DNN method holds high modeling and simulation efficiency in the probabilistic LCF valuation of Turbine blisk.

The efforts of this paper provide a promising measure for the LCF life prediction of turbine blisk from a probabilistic perspective, which is conducive to improve the safety and reliability of aeroengine and airplanes under operation by monitoring health status and residual useful life.

Acknowledgements

This paper is co-supported by National Natural Science Foundation of China (Grant No. 52375237), National Science and Technology Major Project (Grant J2022-IV-0012), Shanghai Belt and Road International Cooperation Project of China (Grant No. 20110741700), China Postdoctoral Science Foundation (Grant No. 2021M700783) and Research Grants Council of the Hong Kong SAR of China (PolyU 15209520). The authors would like to thank them.

References

[1] C.W. Fei, H.T. Liu, S.L. Li, H. Li, L.Q. An, C. Lu, Dynamic parametric modeling-based model updating strategy of aeroengine casings, Chin. J. Aeronaut. 34 (12) (2021) 145−457.
[2] C. Lu, C.W. Fei, H. Li, H.T. Liu, Q. L, An, Moving extremum surrogate modeling strategy for dynamic reliability estimation of turbine blisk with multi-physics fields, Aero. Sci. Technol. 106 (2020) 106112.
[3] Y.M. Temis, Mathematical simulation of low cycle fatigue of high-loaded engine parts, Propuls. Power Res. 7 (4) (2018) 277−287.
[4] R. Yuan, D. Liao, S.P. Zhu, Z.Y. Yu, J. Correia, A. De Jesus, Contact stress analysis and fatigue life prediction of turbine disc−blade attachment with fir−tree tenon structure, Fatig. Fract. Eng. Mater. Struct. 44 (4) (2021) 1014−1026.
[5] N. He, P.F. Feng, Z.W. Li, L.G. Tan, T. Pang, Y.Z. Chen, C. Yang, Fatigue life prediction of centrifugal fan blades in the ventilation cooling system of the high-speed-train, Eng. Fail. Anal. 124 (2021) 105373.
[6] K. Ziane, A. Ilinca, S.S. Karganroudi, M. Dimitrova, Neural network optimization algorithms to predict wind turbine blade

fatigue life under variable hygrothermal conditions, Eng 2 (3) (2021) 278−295.
[7] X. Zhao, D. Ru, P. Wang, L. Gan, H. Wu, Z. Zhong, Fatigue life prediction of a supercritical steam turbine rotor based on neural networks, Eng. Fail. Anal. 127 (2021) 105435.
[8] C.W. Fei, H. Li, H.T. Liu, C. Lu, L.Q. An, L. Han, Y.J. Zhao, Enhanced network learning model with intelligent operator for the motion reliability evaluation of flexible mechanism, Aero. Sci. Technol. 107 (2020) 106342.
[9] C. Zhang, J. Wei, H. Jing, C. Fei, W. Tang, Reliability-based low fatigue life analysis of turbine blisk with generalized regression extreme neural network method, Materials 12 (9) (2019) 1545.
[10] C. Lu, Y.W. Feng, C.W. Fei, S.Q. Bu, Improved decomposed-coordinated Kriging modeling strategy for dynamic probabilistic analysis of multi-component structures, IEEE Trans. Reliab. 69 (2) (2020) 440−457.
[11] C. Lu, H. Li, L. Han, B. Keshtegar, C.W. Fei, Bi-iterative moving enhanced model for probability-based transient LCF life prediction of turbine blisk, Aero. Sci. Technol. 132 (2023) 107998.
[12] C. Lu, C.W. Fei, Y.W. Feng, Y.J. Zhao, X.W. Dong, Probabilistic analyses of structural dynamic response with modified Kriging-based moving extremum framework, Eng. Fail. Anal. 125 (2021) 105398.
[13] C. Lv, J. Chang, W. Bao, D. Yu, Recent research progress on air-breathing aero-engine control algorithm, Propuls. Power Res. 11 (1) (2022) 1−57.
[14] A. Basudhar, S. Missoum, Adaptive explicit decision functions for probabilistic design and optimization using support vector machines, Comput. Struct. 86 (19−20) (2008) 1904−1917.
[15] J. Kang, Z. Wang, C. Guedes Soares, Condition-based maintenance for offshore wind turbines based on support vector machine, Energies 13 (14) (2020) 3518.
[16] S.T. Kandukuri, J.S.L. Senanyaka, K.G. Robbersmyr, A two-stage fault detection and classification scheme for electrical pitch drives in offshore wind farms using support vector machine, IEEE Trans. Ind. Appl. 55 (5) (2019) 5109−5118.
[17] B. Keshtegar, M. Bagheri, C.W. Fei, C. Lu, O. Taylan, D.K. Thai, Multi-extremum modified response basis model for nonlinear response prediction of dynamic turbine blisk, Eng. Comput. 38 (2022) 1243−1254.
[18] H. Gao, A. Wang, G. Bai, C. Wei, C. Fei, Substructure-based distributed collaborative probabilistic analysis method for low-cycle fatigue damage assessment of turbine blade-disk, Aero. Sci. Technol. 79 (2018) 636−646.
[19] I. Ubulom, Influence of fluid-structure interaction modelling on the stress and fatigue life evaluation of a gas turbine blade, Proc. Inst. Mech. Eng. A J. Power Energy 235 (5) (2021) 1019−1038.
[20] L. Han, C. Chen, T.Y. Guo, C. Lu, C.W. Fei, Y.J. Zhao, Y. Hu, Probability-based service safety life prediction approach of raw and treated turbine blades regarding combined cycle fatigue, Aero. Sci. Technol. 110 (2021) 106513.
[21] P. Yue, J. Ma, H. Huang, Y. Shi, J.W. Zu, Threshold damage-based fatigue life prediction of turbine blades under combined high and low cycle fatigue, Int. J. Fatig. 150 (2021) 106323.
[22] J. Huo, D. Sun, H. Wu, W. Wang, Multi-axis low-cycle creep/fatigue life prediction of high-pressure turbine blades based on a new critical plane damage parameter, Eng. Fail. Anal. 106 (2019) 104159.
[23] D. Cazin, S. Braut, Ž. Božić, R. Žigulić, Low cycle fatigue life prediction of the demining tiller tool, Eng. Fail. Anal. 111 (2020) 104457.
[24] M. Banaszkiewicz, The low-cycle fatigue life assessment method for online monitoring of steam turbine rotors, Int. J. Fatig. 113 (2018) 311−323.
[25] Z. Zhan, H. Li, Machine learning based fatigue life prediction with effects of additive manufacturing process parameters for printed SS 316L, Int. J. Fatig. 142 (2021) 105941.
[26] J. Gao, Z. An, H. Kou, Fatigue life prediction of wind turbine rotor blade composites considering the combined effects of stress amplitude and mean stress, Proc. Inst. Mech. Eng. O J. Risk Reliab. 232 (6) (2018) 598−606.
[27] L.K. Song, G.C. Bai, C.W. Fei, Dynamic surrogate modeling approach for probabilistic creep-fatigue life evaluation of turbine disks, Aero. Sci. Technol. 95 (2019) 105439.
[28] S.P. Zhu, Q. Liu, Q. Lei, Q. Wang, Probabilistic fatigue life prediction and reliability assessment of a high pressure turbine disc considering load variations, Int. J. Damage Mech. 27 (10) (2018) 1569−1588.
[29] D. Xu, C. Wen, J. Liu, Wind turbine blade surface inspection based on deep learning and UAV-taken images, J. Renew. Sustain. Energy 11 (5) (2019) 053305.
[30] H. Liu, Z. Zhang, H. Jia, Q. Li, Y. Liu, J. Leng, A novel method to predict the stiffness evolution of in-service wind turbine blades based on deep learning models, Compos. Struct. 252 (2020) 112702.
[31] K. Tao, J. Zhu, Z. Cheng, D. Li, Artificial neural network analysis of the Nusselt number and friction factor of hydrocarbon fuel under supercritical pressure, Propuls. Power Res. 11 (3) (2022) 325−336.
[32] X. Yang, Y. Zhang, W. Lv, D. Wang, Image recognition of wind turbine blade damage based on a deep learning model with transfer learning and an ensemble learning classifier, Renew. Energy 163 (2021) 386−397.
[33] W. Yu, S. Huang, W. Xiao, Fault diagnosis based on an approach combining a spectrogram and a convolutional neural network with application to a wind turbine system, Energies 11 (10) (2018) 2561.
[34] J.R. Jiang, J.E. Lee, Y.M. Zeng, Time series multiple channel convolutional neural network with attention-based long short-term memory for predicting bearing remaining useful life, Sensors 20 (1) (2020) 166.
[35] S. Zare, M. Ayati, Simultaneous fault diagnosis of wind turbine using multichannel convolutional neural networks, ISA (Instrum. Soc. Am.) Trans. 108 (2021) 230−239.
[36] S. Sony, K. Dunphy, A. Sadhu, M. Capretz, A systematic review of convolutional neural network-based structural condition assessment techniques, Eng. Struct. 226 (2021) 111347.
[37] P. Wang, L. Song, Y. Hao, H. Wang, S. Li, L. Cui, A light intelligent diagnosis model based on improved online dictionary learning sample-making and simplified convolutional neural network, Measurement 183 (2021) 109813.
[38] P.A. Kulkarni, A.S. Dhoble, P.M. Padole, Deep neural network-based wind speed forecasting and fatigue analysis of a large composite wind turbine blade, Proc. IME C J. Mech. Eng. Sci. 233 (8) (2019) 2794−2812.
[39] W.J. Veloz Parra, Probabilistic approach for fatigue life estimation of wind turbine blades using deep neural network, Normandie (2020).
[40] J. Xia, Y. Feng, C. Lu, C. Fei, X. Xue, LSTM-based multi-layer self-attention method for remaining useful life estimation of mechanical systems, Eng. Fail. Anal. 125 (2021) 105385.
[41] L. Zou, Y. Li, F. Xu, An adversarial denoising convolutional neural network for fault diagnosis of rotating machinery under noisy environment and limited sample size case, Neurocomputing 407 (2020) 105−120.
[42] D. Li, L. Qiu, K. Tao, J. Zhu, Artificial intelligence aided design of film cooling scheme on turbine guide vane, Propuls. Power Res. 9 (4) (2020) 344−354.
[43] C. Xiao, Z. Liu, T. Zhang, X. Zhang, Deep learning method for fault detection of wind turbine converter, Appl. Sci. 11 (3) (2021) 1280.
[44] D. Meng, M. Liu, S. Yang, H. Zhang, R. Ding, A fluid-structure analysis approach and its application in the uncertainty-based multi-disciplinary design and optimization for blades, Adv. Mech. Eng. 10 (6) (2018) 1687814018783410.
[45] X. Liu, H. Wang, Q. Wu, Y. Wang, Uncertainty-based analysis of random load signal and fatigue life for mechanical structures, Arch. Comput. Methods Eng. (2021) 1−21.
[46] H. Gao, C. Fei, G. Bai, L. Ding, Reliability-based low-cycle fatigue damage analysis for turbine blade with thermo-structural interaction, Aero. Sci. Technol. 49 (2016) 289−300.

[47] C.Y. Zhang, C. Lu, C.W. Fei, L.J. Liu, Y.S. Choy, X.G. Su, Multi-object reliability analysis of turbine blisk with multidiscipline under multiphysical field interaction, Adv. Mater. Sci. Eng. 2015 (2015) 649046.

[48] S.P. Zhu, H.Z. Huang, W. Peng, H.K. Wang, Probabilistic physics of failure-based framework for fatigue life prediction of aircraft gas turbine discs under uncertainty, Reliab. Eng. Syst. Saf. 146 (2016) 1−12.

[49] J.A.M. Pinho da Cruz, J.D.M. Costa, L.F.P. Borrego, J.A. M Ferreira, Fatigue life prediction in AlMgSi1 lap joint weldments, Int. J. Fatig. 22 (7) (2000) 601−610.

[50] J.D. Morrow, Cyclic Plastic Strain Energy and Fatigue of Metals, Internal Friction, Damping, and Cyclic Plasticity, ASTM International, 1965, pp. 45−87.

[51] C. Zhang, J. Wei, H. Jing, C. Fei, W. Tang, Reliability-based low fatigue life analysis of turbine blisk with generalized regression extreme neural network method, Materials 12 (9) (2019) 1545.

[52] L. Han, C. Chen, T. Guo, C. Lu, C. Fei, Y. Zhao, Y. Hu, Probability-based service safety life prediction approach of raw and treated turbine blades regarding combined cycle fatigue, Aero. Sci. Technol. 110 (2021) 106513.